Solution behaviors and self-assembly of polyoxometalates as models of macroions and amphiphilic polyoxometalate-organic hybrids as novel surfactants

ARTICLE *in* CHEMICAL SOCIETY REVIEWS · AUGUST 2012

Impact Factor: 33.38 · DOI: 10.1039/c2cs35176e · Source: PubMed

3 AUTHORS:

Panchao Yin
Oak Ridge National Laboratory
46 PUBLICATIONS **1,269** CITATIONS
SEE PROFILE

Dong Li
Carnegie Mellon University
22 PUBLICATIONS **452** CITATIONS
SEE PROFILE

Tianbo Liu
University of Akron
144 PUBLICATIONS **3,924** CITATIONS
SEE PROFILE

Chem Soc Rev

Cite this: *Chem. Soc. Rev.*, 2012, **41**, 7368–7383

www.rsc.org/csr

TUTORIAL REVIEW

Solution behaviors and self-assembly of polyoxometalates as models of macroions and amphiphilic polyoxometalate–organic hybrids as novel surfactants†

Panchao Yin, Dong Li and Tianbo Liu*

Received 11th May 2012
DOI: 10.1039/c2cs35176e

Large, hydrophilic polyoxoanions with high solubility in water and/or other polar solvents demonstrate unique solution behavior by self-assembling into single layer, hollow, spherical "blackberry" structures, which is obviously different from small, simple ions. These macroions cannot be treated as insoluble colloidal suspensions because they form stable "real solutions". Counterion-mediated attraction is considered as the main driving force for the self-assembly behavior. The size disparity between the macroions and their counterions results in macroion–counterion pairing which leads to the inter-macroanionic attraction. The blackberries, with robust membranes semi-permeable to cations, can adjust their size accurately and reversibly in response to the change of solvent polarity and charge density of individual macroions. The inorganic macroions with well-defined size, shape, mass, charge density, but no intramolecular interactions, are ideal model systems to study the intermolecular interactions in polyelectrolyte and bio-macromolecular solutions. The blackberry structures show certain similarities to spherical viral capsids, from the overall structure to the formation kinetics. More amazingly, these inorganic macroions demonstrate some features usually believed to belong only to complex biological molecules, such as the self-recognition in dilute solutions. Meanwhile, polyoxometalates-based organic–inorganic hybrid materials demonstrate amphiphilic properties by self-assembling into vesicles and reverse vesicles in polar and non-polar solvents, respectively, and form monolayer at the water/air interface. Different from conventional amphiphiles, these hybrids show pH-dependent and counterion-dependent self-assembly behaviors with controllable functionality, *e.g.* fluorescence and catalytic activity, due to the high and tunable charges and the functionalities of POM polar head groups.

1. Introduction

Polyoxometalates (POMs), a large group of metal oxide clusters, represent some of the largest inorganic molecules known so far and have broad applications as catalysts, photo-electronic/magnetic materials, and biologically active materials.[1,2] The POMs are formed by linking metal oxide polyhedra (MO_x, M = Mo, W, V, and Nb; x = 4–7, *e.g.* the different colors of the POMs in Table 1 represent different types of metal oxide polyhedra; light blue, MoO_7 pentagon bi-pyramid polyhedron; dark blue, MoO_6 octahedron; yellow, FeO_6 octahedron; light green, CrO_6 octahedron; dark green, VO_6 octahedron) with each other through corner-, edge-, or face-sharing manner, which enable chemists to build POMs with different topologies and sizes.[2] The performance of POM-based devices and materials depends strongly on their self-assembly structures at different scales including nano-, micro-, and framework structures.[3] Moreover, the nano-scaled, uniform POM molecular clusters may also be applied as valuable model systems to address some fundamental scientific issues, some of them are covered in this review.[4]

Due to the excess of oxo ligands over metal ions, POMs are usually highly negatively charged, *i.e.*, they exist as soluble macroanions in solution. Such macroions have well-defined molecular structures, uniform shapes, tunable charges and no intra-molecular charge interactions, and demonstrate completely different behaviors than regular small ions or large, unstable colloidal suspensions. These polyoxoanions are ideal models for understanding the broadly defined macroionic solutions including polyelectrolytes and biomacromolecular systems, *e.g.*, the interaction between DNA and proteins and the formation of virus capsids.[4,5] This is summarized in the first part of this review.

Department of Chemistry, Lehigh University, 6 E Packer Avenue, Bethlehem, US. E-mail: liu@lehigh.edu; Fax: +1 6107 582935; Tel: +1 6107 586536

† Part of a themed issue covering the latest developments in polyoxometalate science.

Meanwhile, organic functional groups can be covalently grafted to the surface of POMs, resulting in a new type of amphiphilic hybrid materials.[6–8] The solvophobic interaction of the amphiphilic molecules in appropriate solvents can trigger the formation of micelles, vesicles, and reverse-vesicle structures,[9–17] which improves the compatibility of the POMs in organic media. This will be the topic of the second part of this review.

2. Solution behavior of POM macroions

The past decades witness the significant developments in the synthesis of giant POMs with sizes ranging from *ca.* 2 nm to 6 nm (Table 1).[18–25] From physical chemists' point of view, these macroanions are valuable models to understand the transition solution behaviour from simple ionic solution (*e.g.* NaCl solutions, described by Debye–Hückel theory) and colloidal suspensions (Derjaguin–Landau–Verwey–Overbeek theory, or DLVO theory).[4]

2.1. The discovery of the self-assembly of POM macroanions

Large, anionic POMs were observed to slowly form large structures in aqueous solution even though the POMs were highly soluble.[27] Laser light scattering (LLS), a powerful technique in analyzing particle or polymer solutions, is used to monitor the dilute POM solutions. By measuring the scattered intensity from solutions at different scattering angles, static light scattering (SLS) can be used to determine the average molecular weight ($\overline{M_w}$) and radius of gyration (R_g) of the aggregates. Dynamic light scattering (DLS) measures the intensity–intensity time correlation function from the scattered light, which is analyzed by the CONTIN method to calculate the average hydrodynamic radius (R_h) of the particles and the particle size distribution. The LLS results indicated that large structures were detected in various POM solutions, which took a long time to reach equilibrium at room temperature.[4] A typical CONTIN analysis from the DLS study of $\{Mo_{154}\}$ aqueous solution at pH = 3.0 showed the formation of large assemblies with an average R_h of 45 nm and a narrow size distribution (Fig. 1b). The SLS study analyzed by the Zimm plot indicated that the assemblies had an average $\overline{M_w}$ of 2.54×10^7 g mol^{-1} (*ca.* 1150 $\{Mo_{154}\}$) and an average R_g of 45 nm. The relation of $R_h/R_g \approx 1$ for spherical objects (TEM image in Fig. 1a) and the low mass suggested a hollow, single-layered vesicular structure with an average inter-$\{Mo_{154}\}$ distance of $\sim$0.9 nm. Since $\{Mo_{154}\}$ was fully hydrophilic, the assemblies were formed due to different driving forces from the surfactant vesicles where hydrophobic interaction was critical. A nickname "blackberry" was given to the new aggregates due to the similarities between the two species (Fig. 1c).[26] The free-energy favored stable blackberry structures have been observed in appropriate polar solvents of different POM macroanions.[4]

2.2. Driving forces of the self-assembly behavior

The blackberries represent a new type of self-assembled structures in solution, formed by hydrophilic ions with large size and moderate charges. The most critical issue is the driving forces behind the assembly process which brings the like-charged macroions together. A simple experiment helps to clarify this issue and distinguish the macroions from other types of solutes. The $\{Mo_{132}\}$ blackberries were detected in 1.0 mg mL^{-1} water–acetone mixed solvents containing 3–70 vol% acetone, with the average R_h of blackberries increasing from 45 to 100 nm with increasing acetone content (Fig. 2).[28] Only discrete $\{Mo_{132}\}$ clusters were found in solutions containing $<$3 vol% or $>$70 vol% acetone, under which circumstances, the discrete macroanions were of very high or very low charge density, respectively.[28] In an acetone-rich solvent, the strong counterion condensation made the effective charge of $\{Mo_{132}\}$ very low (almost neutral). In such a case, $\{Mo_{132}\}$ clusters existed as single clusters. With increasing water content, the effective charge of the macroions increased, which

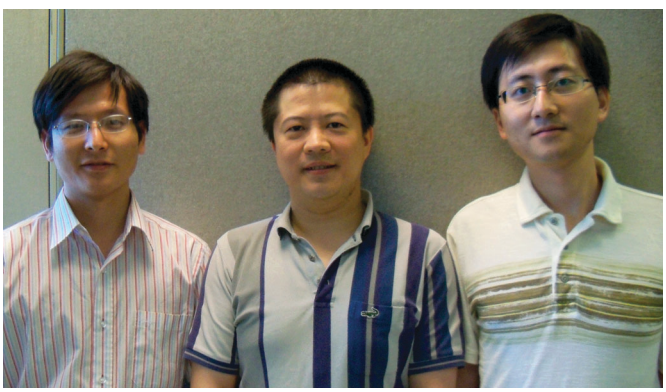

Panchao Yin, Tianbo Liu and Dong Li

Panchao Yin (left) was born in Xiaogan, Hubei province of China in 1987. He studied polymer science and engineering in department of chemical engineering at Tsinghua University (Beijing) and received his BSc in chemical engineering in 2009. He started his PhD studies at Lehigh University in 2009 under the supervision of Prof. Tianbo Liu and works on self-assembly of proteins, macroions, and POM–organic hybrids.

Dong Li (right) was born in Jinan, China, in 1983. He received his BSc from Shandong University in 2006 and MSc from Lehigh University in 2009. He is currently pursuing a PhD in Physical Chemistry under the supervision of Prof. Tianbo Liu. His research focuses on the solution behaviors of macro-cations in solutions and the self-assembly of viral capsids. He is a Constance N. Busch fellowship recipient.

Tianbo Liu (middle) was born in Beijing, China, and received his BS degree in Chemistry from Peking University in 1994. He received his PhD in Chemistry from the SUNY at Stony Brook in 1999, under the guidance of Professor Benjamin Chu. During this time he studied block copolymer solutions by using scattering techniques. After spending two more years in the same group as a postdoctoral associate, he started his independent research career at Physics Department, Brookhaven National Laboratory. In Jan 2005 he moved to Lehigh University, where he is currently professor of Chemistry. His laboratory focuses on understanding the fundamental behaviour of complex solutions, especially hydrophilic macroions, inorganic–organic hybrid surfactants and other colloidal and biological systems. In Jan. 2013 he will move to Department of Polymer Sciences, The University of Akron as A. Schulman Chair Professor.

Table 1 Information on the structure, charge density, and self-assembly behavior of macro-polyoxoanions in aqueous solutions

Polyoxoanion	$\{Mo_{72}Fe_{30}\}$			$\{Mo_{72}Cr_{30}\}$	$\{Mo_{154}\}$	$\{Cu_{20}P_8W_{48}\}$	$\{P_4Y_9W_{43}\}$	$\{Mo_{132}\}$	$\{Mo_{72}V_{30}\}$
Molecular structure									
Negative charge	0–1	1–29		5	15	25	30	42	31
Size (nm)	2.5			2.5	3.6 × 1.2	2.2 × 1.1	4 × 2 × 2	2.9	2.5
Charge density (nm^{-2})	0–0.051	0.051–1.477 2.9	Unstable	0.255	0.543	1.291	1.08	1.590	1.579
	pH < 2.9	< pH < 6.6	pH > 6.6						
Self-assembly in aqueous solution	No	Yes	Unstable	Yes	Yes	Yes	Yes	Yes at high conc.	No
R_h of Blackberry (nm)		48–15		60	45	38	46		

	Formula	Ref.
$\{Mo_{72}Fe_{30}\}$	$[Mo^{VI}{}_{72}Fe^{III}{}_{30}O_{252}(CH_3COO)_{12}\{Mo_2O_7(H_2O)\}_2\{H_2Mo_2O_8(H_2O)\}(H_2O)_{91}]\cdot ca.\ 150H_2O$	21
$\{Mo_{72}Cr_{30}\}$	$[\{Na(H_2O)_{12}\}\subset\{Mo^{VI}{}_{72}Cr^{III}{}_{30}O_{252}(CH_3COO)_{19}(H_2O)_{94}\}]\cdot ca.\ 120H_2O$	25
$\{Mo_{154}\}$	$Na_{15}[Mo_{154}O_{462}H_{14}(H_2O)_{70}]_{0.5}[Mo_{152}O_{457}H_{14}(H_2O)_{68}]_{0.5}\cdot ca.\ 400H_2O$	18
$\{Cu_{20}P_8W_{48}\}$	$K_{12}Li_{13}[Cu_{20}Cl(OH)_{24}(H_2O)_{12}(P_8W_{48}O_{184})]\cdot 22H_2O$	24
$\{P_4Y_9W_{43}\}$	$K_{15}Na_6(H_3O)_9[(PY_2W_{10}O_{38})_4(W_3O_{14})]\cdot 39H_2O$	23
$\{Mo_{132}\}$	$(NH_4)_{42}[\{(Mo^{VI})Mo^{V}{}_{15}O_{21}(H_2O)_6\}_{12}\{Mo_2O_4(CH_3COOH)\}_{30}]\cdot ca.\ 300H_2O\cdot ca.\ 10CH_3COONH_4$	19
$\{Mo_{72}V_{30}\}$	$Na_8K_{14}(VO)_2[\{(Mo^{VI})Mo^{VI}{}_5O_{21}(H_2O)_3\}_{10}\{(Mo^{VI})Mo^{VI}{}_5O_{21}(H_2O)_3(SO_4)\}_2\{V^{IV}O(H_2O)\}_{20}\{V^{IV}O\}_{10}(\{KSO_4\}_5)_2]\cdot ca.\ 150H_2O$	22

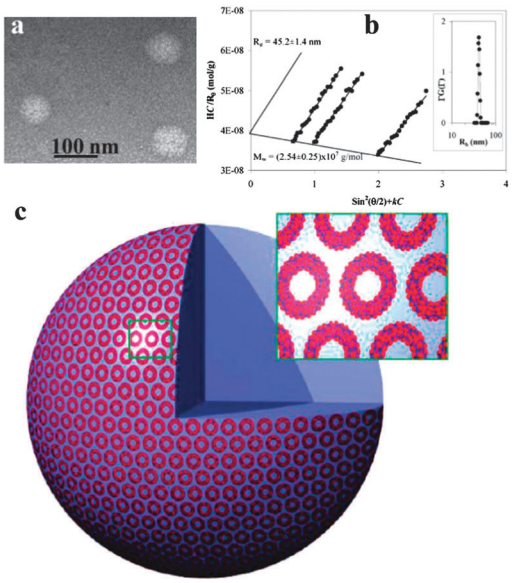

Fig. 1 (a) TEM image on dilute aqueous solution of $\{Mo_{154}\}$ macroions showing the existence of spherical, ~45 nm radius assemblies. (b) Zimm plot based on the SLS study of the $\{Mo_{154}\}$ aqueous solutions at pH = 3; (inset) CONTIN analysis on the DLS study of the same solution. (c) Schematic plot showing the supramolecular blackberry structure formed by $\{Mo_{154}\}$ macroions in aqueous solution. Reprinted with permission from ref. 26. Copyright 2003 Nature Publishing Group.

should increase the electrostatic repulsion between individual $\{Mo_{132}\}$ macroanions. Instead, the $\{Mo_{132}\}$ macroanions started to attract strongly each other and form blackberries. This observation rules out the possibility that van der Waals forces are the major driving forces for the self-assembly process.[4]

On the other hand, in various macroionic solutions, the blackberry size shows linear relationship with the inverse of

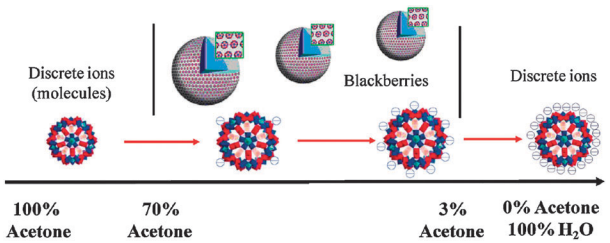

Fig. 2 Transition from discrete macroions (molecules) to blackberries, then to discrete macroions due to the change of solvent content for 1.0 mg mL^{-1} $\{Mo_{132}\}$ in water–acetone mixed solvents. Reprinted with permission from ref. 28. Copyright 2007 American Chemical Society.

the dielectric constant of the solvent, implying a charge-regulated self-assembly process (Fig. 3).[29] The assumption of such a 'charge-regulated' self-assembly process was further confirmed by the pH-controlled self-assembly behavior of $\{Mo_{72}Fe_{30}\}$. $\{Mo_{72}Fe_{30}\}$ can be treated as a weak nano-acid by partially deprotonating the 30 water ligands coordinated to the 30 Fe(III) centers on its surface.[21] The chemical equilibrium for deprotonation and protonation of $\{Mo_{72}Fe_{30}\}$ could be tuned by changing the solution pH, which controlled the net charge of $\{Mo_{72}Fe_{30}\}$.[30] No aggregates formed in solution with pH < 2.9,[30] suggesting that the charge density of $\{Mo_{72}Fe_{30}\}$ was too low to form blackberry structures, which not only ruled out the major contribution of van der Waals forces, but also confirmed the importance of the charge effect in blackberry formation.[4]

2.3. Source of counter-ion mediated interaction

The single ion–blackberry–single ion transition shown above might be explained as that the counterion-mediated attraction is not strong enough to overcome the repulsion between POMs with very high charges, while POMs with very low charges are

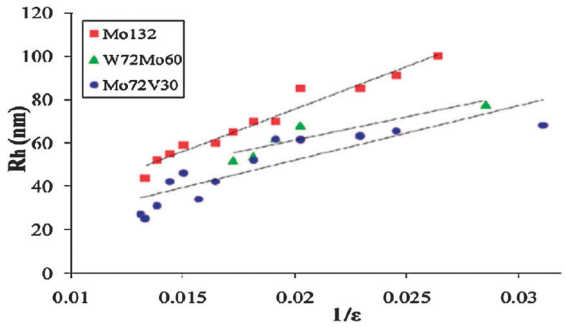

Fig. 3 Plot of the average blackberry radius (in R_h) *versus* the inversed dielectric constant ($1/\varepsilon$) of the solvent for various POM macroions in water–acetone mixed solvents. Linear relationship roughly follows for these systems. Reprinted with permission from ref. 4. Copyright 2010 American Chemical Society.

not able to hold counterions as ion-pairing structures, which will largely reduce the attractive force.[4] The proper charge density range favoring the self-assembly behavior is summarized in Table 1. Basically, the charge density of macroions with a size of 2–4 nm should be within the range of 0.051–1.471 nm^{-2} in order to be able to self-assemble into blackberry structures in aqueous solution. Obviously, this charge density range will vary with the macroionic size.

By realizing the importance of charge in the blackberry formation and the significance, but not dominant size disparity between macroions and their counterions, we tried to seek for the possible contribution of the counterion-mediated attraction as the possible driving forces. Similar cases were reported in polyelectrolyte and biomacromolecular (proteins and DNAs) solutions, although usually multivalent counterions are needed (in our current cases monovalent counterions already can achieve this).[31] Inspired by the formation of bound pairs of highly charged polystyrene latex particles in the aqueous environment, Sogami and Ise confirmed the counterion-mediated attraction between like-charged colloidal particles experimentally and theoretically (although still controversial in colloid community since van der Waals forces among colloidal particles are so dominant).[32]

Due to their high charges and size disparity between them and their counterions, POM macroions can strongly associate with their counterions and form ion-pairs, which are considered to play a significant role in the formation of blackberry structures.

2.3.1. Small-angle X-ray scattering. Small-angle X-ray scattering (SAXS) can be used to explore the information on the shape and size of macromolecules, characteristic distances of partially ordered materials, pore sizes, *etc*.[33] SAXS is suitable for studying the POMs in dilute solution because of their giant sizes and well-defined structures.[34,35] Within the appropriate concentration range, SAXS curves are quite sensitive to the changes of radius of gyration (R_g) and the shape of POM macroanions.[34,35] Either counterion association around POMs or the self-assembly of POMs will lead to noticeable change in SAXS curves, which can be further quantitatively interpreted by calculating the R_g value and the distance pair distribution functions.[34,35]

2.3.2. Counterion distribution around polyoxoanions. $\{Mo_{72}V_{30}\}$ stays as discrete anions in dilute aqueous solution due to its high charge density, making it a good model for studying counterion distribution around macroanions.[34,36]

$\{Mo_{72}V_{30}\}$ macroanions theoretically carry $\sim$31 negative charges with the counterions being 14 K^+, 8 Na^+, 2 VO^{2+}, and 5 H^+ in their very dilute solutions (proton might be partially associated with surface oxo ligands). The corresponding SAXS curve identified several peaks which could be fit well by the form factor of single $\{Mo_{72}V_{30}\}$ clusters. The distance pair distribution $p(r)$, the probability of finding the vector length r in a molecule, could be generated from the Moore analysis of the SAXS curve to provide a physically meaningful description of the particle morphology. For $\{Mo_{72}V_{30}\}$ in dilute aqueous solution, the $p(r)$ curves shown in Fig. 4 (top) correspond to single $\{Mo_{72}V_{30}\}$ clusters (a core–shell spherical particle with a maximum linear dimension of 26 Å) without counterion association around macroions. However, when the concentration was over 0.052 mM or a certain amount of acetone was introduced into the solution, another new peak appeared (centered at $\sim$30 Å and extended the effective distribution to $\sim$34 Å) in the $p(r)$ plot (Fig. 4, bottom). The original distribution remained unchanged, suggesting that the macroions still existed as discrete ions. This additional peak suggested that some metal counterions were closely associated with the macroions and distributed 0.2–0.9 nm to the surface of macroions. This peak became more and more significant with increasing POM concentration or acetone content. Meanwhile, Guinier plots indicated that the average R_g value of the $\{Mo_{72}V_{30}\}$ macroions also increased accordingly. The appearance of the peak

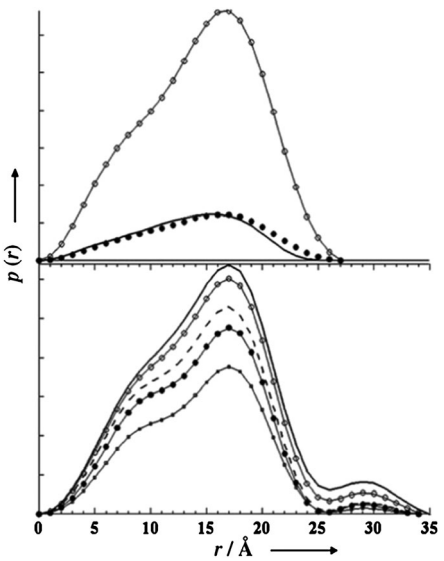

Fig. 4 Top: distance distribution functions based on calculated and experimental scattering data for $\{Mo_{72}V_{30}\}$ obtained by using an indirect Fourier transform of the primary SAXS data. (○): 0.052 mm $\{Mo_{72}V_{30}\}$, (●): 0.013 mm $\{Mo_{72}V_{30}\}$, (—): $\{Mo_{72}V_{30}\}$ calculated. Bottom: experimental distance distributions for 0.26 mm $\{Mo_{72}V_{30}\}$ in water and acetone–water mixed solvents with various acetone contents (in vol%). (—): 75% acetone–water, (○): 65% acetone–water, (---): 45% acetone–water, (···): 10% acetone–water, (□): in pure water. Reprinted with permission from ref. 34. Copyright 2009 Wiley-VCH.

due to associated counterions was consistent with the appearance of the blackberry structures in solution, indicating a direct connection between these two issues and the role of counterions in the blackberry formation.[34]

The counterion effect is critical in the current case because the size disparity between the macroions and counterions is obvious, but not significant (like in the case of colloids). In other words, in macroionic solutions, the counterions cannot be treated as point charges (in colloidal suspensions it has no problem) and consequently the hydrated size of the counterions becomes important. This introduces more challenges to theoretical approaches because the mean field approach cannot be applied for the macroionic solutions quantitatively.[4,34]

2.3.3. Counterion exchange around macroanions. The appropriate size disparity between macroions and their counterions also renders the macroions another important feature – it can accurately distinguish monovalent counterions with different hydrated sizes, and has a corresponding preference sequence. In other words, the exchange of monovalent counterions around such macroions can be achieved. A simple observation was the change of blackberry size when a small amount of proper extra salt was added (Fig. 5). For $\{Mo_{72}Fe_{30}\}$, the original counterions were protons. Its blackberry size did not change from the salt-free solutions when 1–20 mM LiCl or NaCl was added. However, when 0.1–10 mM KCl or a small amount of RbCl was added, the blackberry size became considerably larger ($R_h \sim 34.6$ nm and 35.7 nm, respectively). A reasonable explanation is that K^+ and Rb^+ ions (smaller hydrated sizes) could replace the protons around $\{Mo_{72}Fe_{30}\}$, which would increase the attractive force between macroions and lead to larger blackberries, while large hydrated ions such as Li^+ and Na^+ could not replace the protons due to their lower priority.[35]

This speculation was confirmed by isothermal titration calorimetry (ITC) studies. By adding NaCl to the aqueous solution of $\{Mo_{72}Fe_{30}\}$, there was no measurable binding of Na^+ ions to macroions even with the molar ratio of Na^+ to POM of 1000 : 1. The titration curve for KCl indicated that binding between K^+ ions and the $\{Mo_{72}Fe_{30}\}$ macroions was present. 50–60 K^+ were needed for completely saturating the binding sites ($\sim$6) on $\{Mo_{72}Fe_{30}\}$. Instead, $<$10 Rb^+ ions were needed for saturation, suggesting that the binding to $\{Mo_{72}Fe_{30}\}$ macroions was much stronger for Rb^+ than for K^+. The ITC studies provided direct confirmation that the binding strength between $\{Mo_{72}Fe_{30}\}$ and monovalent

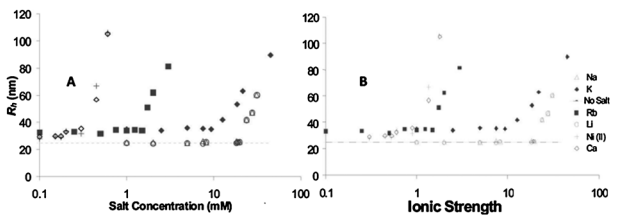

Fig. 5 Change of blackberry size (in R_h) with added chloride salt concentration (A) and total ionic strength (B) for 0.5 mg mL^{-1} $\{Mo_{72}Fe_{30}\}$ solutions. For each added cation salt there is a CSC (critical salt concentration), above which the blackberry size increases with increasing salt concentration. Reprinted with permission from ref. 35. Copyright 2010 American Chemical Society.

cations followed the order of (Li^+, Na^+) $<$ H_3O^+ $<$ K^+ $<$ Rb^+ $<$ Cs^+, which was completely consistent with the observed corresponding blackberry formation processes.[35]

Direct evidence for the counter-cation exchange was obtained from anomalous small-angle X-ray scattering (ASAXS) studies. When Rb^+ was present in $\{Mo_{72}V_{30}\}$ solution, there was an obvious difference between the $I(Q)$ response obtained at different energies. The difference indicated that Rb^+ distributed homogeneously and isotropically around the macroions, which meant that the replacement of K^+ by Rb^+ in $\{Mo_{72}V_{30}\}$ solution was possible. Furthermore, the pH value of the aqueous solution decreased due to the release of more free protons resulting from counterion replacement. The capability of distinguishing different monovalent cations in dilute solution is unique for these hydrophilic macroions.[35]

2.3.4. Water-bridged hydrogen bonding. $\{Mo_{72}Fe_{30}\}$ and $\{Mo_{72}Cr_{30}\}$ are two POMs with the same size and morphology.[21,25] They can be of the same charge density by carefully tuning the pH of their individual aqueous solutions, however, their assembly sizes are very different (even with the same charge density), which implies the existence of another inter-POM force besides charge interaction (Table 1).[36] $\{Mo_{154}\}$, a wheel-shaped molecule with 70 water ligands on its surface, was applied for dielectric relaxation measurements to directly uncover the role of 'the force', hydrogen bonding in the formation of blackberry structures.[37] The conductance-corrected dielectric spectra and difference spectra of a fresh prepared solution and 'aged' solution (two weeks after the preparation) were comparatively studied, which indicated that 'the strength of the hydration extends as cluster association took place with more water molecules being more strongly bound between the wheels and the presence of relatively fewer less strongly bound water molecules'.[37] Simply put, the water can stay between the macroanions with higher viscosity than pure water, which helps to bind the POMs together. However, $\{Mo_{72}Fe_{30}\}$ and $\{Mo_{72}Cr_{30}\}$ were not able to self-assemble into blackberry structures at low pH, suggesting that water-bridged hydrogen bonding might not be the dominant driving force for the blackberry formation, but the force to strengthen the interaction between macroions.[30,36]

2.3.5. Stability of polyoxoanions in salt-containing aqueous solutions. The stability of polyoxoanions and blackberry structures has been explored at high salt concentrations. Basically, the stability of blackberries can be studied in the same way as we do for colloidal systems due to their larger sizes than discrete POM anions. As the fundamental theory in colloid science, DLVO theory reveals that the stability of the colloids depends on the competition between electrostatic repulsion and attractive van der Waals forces. Usually adding extra ions can destabilize the colloidal system since it significantly screens the repulsive interactions. Different types of cations were added to the aqueous solutions of $\{Mo_{72}Fe_{30}\}$ with different concentrations, respectively (Table 2). Precipitation, indication of the instability, can be observed when the concentrations of added salts passed a critical salt concentration (CSC). The monovalent cations with smaller hydrate radii had lower CSC values. The cations with higher valence showed much lower CSC values. Interestingly, there was no such obvious trend among different

Table 2 Critical salt concentrations needed for precipitating $\{Mo_{72}Fe_{30}\}$ blackberries from different $\{Mo_{72}Fe_{30}\}$ concentrations. Reprinted with permission from ref. 38. Copyright 2010 Elsevier

Ion	Critical concentration (mM) 0.1 mg mL^{-1} $\{Mo_{72}Fe_{30}\}$	Critical concentration (mM) 0.25 mg mL^{-1} $\{Mo_{72}Fe_{30}\}$	Critical concentration (mM) 0.5 mg mL^{-1} $\{Mo_{72}Fe_{30}\}$
Li^+	25	50	95
Na^+	8.5	36	70
K^+	6	25	50
Rb^+	0.5	1	4
Cs^+	0.2	0.3	0.5
NH_4^+	2.5	12	27.5
Mg^{2+}	0.25	0.5	1
Ca^{2+}	0.25	0.5	1
Ba^{2+}	0.25	0.5	1
Ni^{2+}	0.25	0.5	1
Al^{3+}	<0.005	0.02	0.05

divalent cations. In this respect, the valence of the divalent cations was so dominant on determining the stability of blackberries which made other factors, *e.g.*, the hydration of the cations, negligible. Macroanionic concentration dependence was found where the stability of the $\{Mo_{72}Fe_{30}\}$ solution increased with increasing macroanionic concentration. This behavior is likely attributed to the close association of monovalent counter-ions around macroions existing in aqueous solution which is facilitated at higher macroionic concentrations. The precipitates from $\{Mo_{72}Fe_{30}\}$ solutions could be re-dissolved in solution (except for solutions containing Cs^+ or Rb^+) when adjusting the solution pH < 1.5 so that the $\{Mo_{72}Fe_{30}\}$ clusters became almost charged neutral and fully protonated.[38]

2.4. Controlling the assembly–disassembly and blackberry size

The assembly and disassembly of the blackberries, as well as the transition between the blackberries with different sizes, can be achieved by properly adjusting the parameters such as the macroionic charge density, solvent polarity, and extra salt concentration.

2.4.1. 'Power on/off' of the self-assembly process and accurately controlling the blackberry size. The charge density of macroions can be tuned by changing the concentration or temperature of the macroionic solutions besides the effect of solution pH and solvent polarity discussed earlier. The charge density is too low for macroions to self-assemble when the pH of 0.5 mg mL^{-1} $\{Mo_{72}Fe_{30}\}$ aqueous solution is <2.9; or for $\{Mo_{132}\}$ in acetone–water solution the acetone content is over 70% vol. The self-assembly process can be triggered by adding base into the aqueous solution of $\{Mo_{72}Fe_{30}\}$, or adding an appropriate amount of water to the acetone–water solution of $\{Mo_{132}\}$.[28,30] On the other hand, the disassembly of the blackberries can be achieved by applying the reverse procedures. $\{Mo_{72}Cr_{30}\}$ shows a similar pH-controlled self-assembly behavior with $\{Mo_{72}Fe_{30}\}$ by displaying the 'switch' point at pH = 2.7.[36] $\{Mo_{72}V_{30}\}$ is able to self-assemble into blackberry within the range 2–90 vol% acetone in acetone–water mixed solvents.[36] Meanwhile, due to the capturing of counterions (ammonium) in the nano-pores on the surface of $\{Mo_{72}Fe_{30}\}$, its charge density is lowered and appropriate for counterion-mediated self-assembly. However, the total scattered intensity dropped, which meant the blackberry disassembled, after mild heating of the solution from room temperature to 40 °C.[39] The 'power off' process can be explained by exceeding the critical charge density of $\{Mo_{72}Fe_{30}\}$ resulting from the temperature enhanced release of the ammonium ions from the pores into bulk solution.[39]

By continuously tuning the pH of the weak acid type POMs' solutions, the solvent polarity of strong electrolyte POMs' solutions or adding cationic surfactants to macroionic solutions in the range that the formation of blackberry can be observed, the charge density of macroanions is supposed to be varied, which shows a significant effect on the assembly size.[4] In the aqueous solution of $\{Mo_{72}Fe_{30}\}$, the blackberry size decreases with increasing pH, from ~50 nm at pH = 3.0 to ~15 nm at pH = 6.0 (Fig. 6).[30] The blackberry size of $\{Mo_{72}Cr_{30}\}$ decreases from 70 to 40 nm within the pH range 2.7–7.0.[36] $\{Mo_{132}\}$ formed blackberry structures in water–acetone mixed solvents containing 3 to 70 vol% acetone, with their average R_h increasing from 45 to 100 nm with increasing acetone content (Fig. 2). The average blackberry size increased linearly with increasing $1/\varepsilon$, with ε being the solvent's dielectric constant (Fig. 3).[28] Similar trends have also been identified in $\{Mo_{72}V_{30}\}$ and $\{W_{72}Mo_{60}\}$ in water–acetone mixed solvents.[29] A charge regulated self-assembly process was given to explain the formation of blackberry, which predicted that the vesicle size is proportional to the inverse of the dielectric constant of the solvent.[29]

Cationic surfactants with long enough alkyl chains can interact with macroanions stoichiometrically and therefore be used to accurately decrease the macroionic effective charge (Fig. 7). A typical study was carried out with $\{Mo_{72}V_{30}\}$, which does not show self-assembly behavior in dilute aqueous solution due to its high charge density.[40] After introducing a small amount of water-soluble cationic surfactants, such as cetyltrimethylammonium bromide (CTAB), trimethyltetradecylammonium chloride (CTAT), dodecyltrimethylammonium bromide (DTAB), and octyltrimethylammonium bromide (OTAB), the charge density of $\{Mo_{72}V_{30}\}$ macroions decreased so that the $\{Mo_{72}V_{30}\}$ macroions entered the blackberry-formation regime (Fig. 7). The average R_h of the blackberries continued to increase with increasing surfactant concentration, as shown in Fig. 7.[40] CTAB and CTAT strongly interacted with the macroions stoichiometrically while shorter OTAB had much weaker interaction with the macroions.[40]

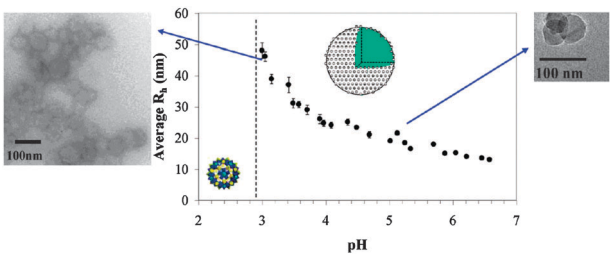

Fig. 6 Average hydrodynamic radii (R_h) of the blackberries formed in 0.5 mg mL^{-1} aqueous solutions of $\{Mo_{72}Fe_{30}\}$ at different pH (adjusted by NaOH or HCl), as measured by DLS at 90° scattering angle. TEM images of aggregates on carbon films formed at pH ~ 3.0 (left; conventional TEM) and pH ~ 4.6 (right; more appropriate cryo-TEM). Reprinted with permission from ref. 30. Copyright 2006 American Chemical Society.

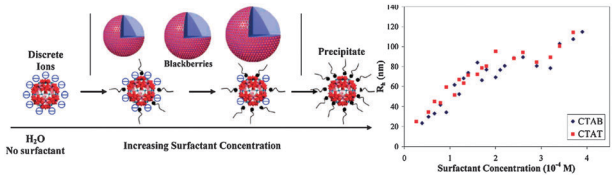

Fig. 7 (left) Gradually introducing alkyl trimethylammonium halide cationic surfactants into the dilute aqueous solution of $\{Mo_{72}V_{30}\}$ clusters can gradually decrease the charge density of the $\{Mo_{72}V_{30}\}$ macroions and induce blackberry formation. The average blackberry size increases with increasing surfactant amount (*i.e.* decreasing charge density of $\{Mo_{72}V_{30}\}$). (right) Average hydrodynamic radius (R_h) of the $\{Mo_{72}V_{30}\}$ blackberries in aqueous solution containing CTAB or CTAT, measured by DLS. The concentration of $\{Mo_{72}V_{30}\}$ is 0.5 mg mL^{-1}, equivalent to a molar concentration of 2.6×10^{-5} M. Reprinted with permission from ref. 40. Copyright 2009 American Chemical Society.

Represented by $\{Mo_{72}V_{30}\}$ and $\{P_4Y_8W_{43}\}$, weak acid salt type POMs carry a considerable amount of charges in crystals but still further deprotonate some surface water ligands when dissolving in a solvent.[34,41] For these macroions, their self-assembly processes can be controlled by either changing the solvent content or changing solution pH (in aqueous solution). Consequently, such POMs are valuable for directly comparing the effects of the solvent content and solution pH on the blackberry size. The yttrium-containing lacunary polyoxotungstate $\{P_4Y_8W_{43}\}$ macroanions could form $R_h \sim 53$ nm blackberries in 0.3 mg mL^{-1} aqueous solution. The blackberry size increased with increasing amount of acetone added into the solution, which was quantitatively similar to the case of $\{Mo_{132}\}$. Changing solution pH could also alter the blackberry size. However, since the pH change only affected the amount of protons released from the macroions, the change of blackberry size due to pH was smaller than the change caused by changing solvent content.[41]

2.4.2. Size limit of the 'macroanions'. The size disparity between highly-charged particles and their counter-ions is considered to be the source for ion-pairing and like-charge interaction.[42] The static charge interaction is stronger than the thermal motion of small counterions, however, weaker than the thermal motion of large particles. In that way, it can hold counterions around the highly charged particles. As a quite important but unsolved issue, what is the critical size of the macroion that can self-assemble into blackberry structures? Currently, the smallest polyoxoanions that were proved to be able to self-assemble are $\{Cu_{20}P_8W_{48}\}$ with size $2.2 \times 2.2 \times 1.1$ nm^3 (Table 1).[43] Further exploration on POMs with different sizes is underway in our lab to determine the critical size.

2.4.3. Controlling the morphology of the assemblies. In the model of blackberry structure, the macroions are supposed to distribute quite homogeneously on the surface although no long-range closed packing is expected or observed (Fig. 1c).[26] Due to the symmetrical molecular structure and isotropic charge distribution of the macroions we have studied, assemblies with 3D symmetry are expected. However, the macroions with asymmetrical molecular structure or anisotropic charge distribution are not able to pack in the same way. The design of macroions with required symmetry and charge distribution might render us the ability to control the morphology and symmetry of assemblies.

Peng and his co-workers have successfully synthesized conjugated polymers with POMs as their side chain or main chain.[45] For the conjugated polymers containing POM-terminal side chains in polar solvents, due to its rigid nature and macroionic properties inherited from the POMs, the polymer single chain existed almost like a 1D rod-like macroion.[44] The rod-shaped polymer did not favor the 3-D symmetrical spherical assemblies. Instead, these 1-D linear "macroions" formed the corresponding 1-D hollow supramolecular structures, *i.e.*, the tube-like morphology in DMSO and acetone, as shown schematically in Fig. 8. The diameter of the tubes became larger with the existence of $ZnCl_2$ or tetramethyl ammonium bromide. However, the thickness of the wall did not change, suggesting the obvious role of counterions and the charge-regulated mechanism for the self-assembly behavior. The addition of tetrapropylammonium bromide and tetrabutyl ammonium bromide was suggested by light scattering results to have no effect on the sizes of the supramolecular structures.[44,46]

The macroions with anisotropic charge distribution can also assemble into non-spherical objects with low symmetry. The tin-12 oxo cluster (Fig. 9), $\{(RSn)_{12}O_{14}(OH)_6\}^{2+}$, first reported in 1989, is an interesting, positively charged organic–inorganic cluster. The football-shaped cluster exhibits two positive charges that are located at the poles of the cluster, defined by the six-coordinated Sn ions and the u^2 ligands.[47,48] Because of the location of the two positive charges, the cluster can interact with dianions to show some interesting assembly behaviors. Very recently, Ribot *et al.* applied pulsed field gradient NMR spectroscopy to probe the anions mediated associative behavior of $\{(RSn)_{12}O_{14}(OH)_6\}^{2+}$. The counterion can only interact with the two poles of the $\{Sn_{12}\}$, which finally direct the formation of a worm-like structure in organic solvents (Fig. 9).[47,48]

2.5. The unique slow self-assembly process *vs.* the virus capsid formation

Blackberries are thermodynamically stable, which is quite different from the colloidal systems.[4,49–52] Different from the

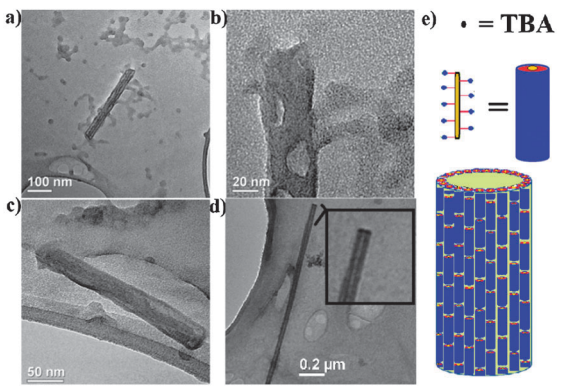

Fig. 8 TEM images for (a) assemblies in acetone; (b) zoom in image of the feature in (a); (c) another rod structure in acetone; (d) assemblies in DMSO (inset: zoom in image of the tube structure). (e) Model for the tube-like assemblies. Reprinted with permission from ref. 44. Copyright 2012 Wiley-VCH.

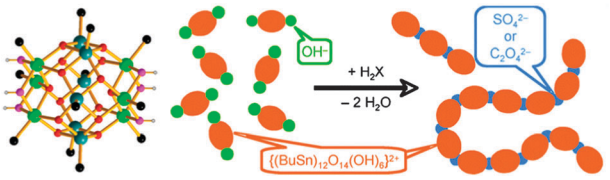

Fig. 9 (left) Molecular structure of $\{(RSn)_{12}O_{14}(OH)_6\}^{2+}$. (Six-coordinated tin, green; five-coordinated tin, teal; u_3-oxo, red; u_2-oxo, purple; R, black; hydrogen, gray). (right) The formation of large aggregates induced by dianions. Reprinted with permission from ref. 48. Copyright 2010 American Chemical Society.

comparatively fast self-assembly of amphiphilic molecules, the macroanions need a long period of time, sometimes even months at room temperature, to reach the equilibrium state.[4,43,53] The unique slow self-assembly process has been studied by long-time monitoring results and kinetic studies, which shared similarities with the self-assembly of virus capsid proteins.[4]

2.5.1. The kinetic properties of the self-assembly. The slow blackberry formation under certain circumstances enables detailed study on the mechanism of the assembly. Fig. 10 demonstrates a typical SLS and DLS study on the formation of $\{Mo_{72}Fe_{30}\}$ blackberries in aqueous solution at different macroionic concentrations. The scattered intensity recorded by SLS continued to increase with time, suggesting the continuous formation of large structures in solution. At the same time, DLS studies indicated that there exist two different types of particles in solution: discrete macroions ($R_h \sim 1.2$ nm) and blackberries ($R_h \sim 25$ nm). The first peak became smaller and smaller while the second one grew larger with time, indicating that the discrete macroions were continuously forming blackberries while the average blackberry size remained almost unchanged during the whole process. Combining the above information, we concluded that the formation mechanism of the blackberry should follow the upper route in Fig. 11. That is, at the beginning, the unimers slowly associated into dimers (and oligomers). This was the rate-determining step. Once enough oligomers were available, they quickly assembled into blackberries at their favoured size.[43,53]

The slow blackberry formation is attributed to the high energy barrier for the transition from single macroions to blackberries. Time-resolved SLS studies were used to determine the initial "reaction" rates in $\{Mo_{72}Fe_{30}\}$ aqueous solutions at

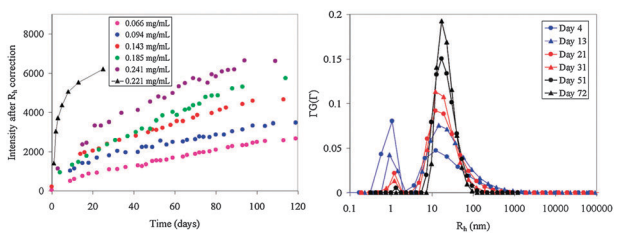

Fig. 10 (left) Change of total scattered intensity of $\{Mo_{72}Fe_{30}\}$ solutions at 90° scattering angle. All solutions were kept at 25 °C except one at 45 °C (the data shown by black triangle). (right) CONTIN analysis of the DLS study on $\{Mo_{72}Fe_{30}\}$ aqueous solution at different times. Reprinted with permission from ref. 53. Copyright 2005 American Chemical Society.

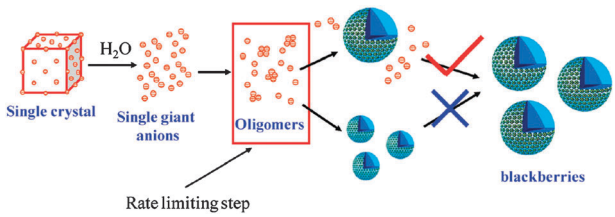

Fig. 11 Possible mechanisms of $\{Mo_{72}Fe_{30}\}$ blackberry formation in dilute aqueous solution. The upper mechanism has been proven to be correct based on SLS and DLS results, while the bottom mechanism can be ruled out. Adapted with permission from ref. 43 and reprinted with permission from ref. 5. Copyright 2010 American Chemical Society.

different temperatures. The 'rate' could be significantly enhanced by increasing the temperature of the solutions. By using the Arrhenius equation $\ln(k) = -E_a/RT + \ln A$, the activation energy of the oligomer formation could be calculated to be $\sim 115 \pm 8$ kJ mol^{-1}, which was indeed very high (Fig. 12).[53]

2.5.2. Lag phase during the blackberry formation. In aqueous solution containing no or small amount of extra monovalent cations (*e.g.* NaCl, NaBr, NaI, and Na_2SO_4 at concentrations of 0.017 mol L^{-1}), the $\{Mo_{72}Fe_{30}\}$ blackberry formation process, recorded by SLS studies as the time-resolved intensity curve, showed a linear relationship with time, similar to a first-order reaction.[53] However, a lag phase was also observed in the SLS studies of the dilute solutions of $\{Cu_{20}P_8W_{48}\}$[43] and $\{Mo_{72}Fe_{30}\}$[53] (in minutes). This lag phase became significant when the extra salt concentration was higher or introducing glycerol, a viscous and water-miscible solvent, as shown in Fig. 13. Overall, the whole kinetic curve is sigmoidal.[54]

The sigmoidal curve for a self-assembly process has also been reported in other systems such as virus capsid formation (Fig. 13),[55] ester hydrolysis, vesicle formation, and nanoparticle preparation. In general, it is considered to be a typical feature of a two-step process: in the initial lag period, the "reaction" begins with the slow formation of oligomer nucleus; once the amount of the rate limiting nucleus has reached a critical value, subsequent oligomers or monomers are quickly added to the growing assembly structures at a time until it is complete.[54]

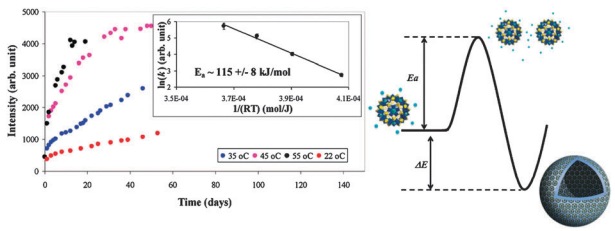

Fig. 12 (left) Increment of the scattered intensity (I) from 0.5 mg mL^{-1} $\{Mo_{72}Fe_{30}\}$–H_2O solutions at different temperatures (22, 35, 45, and 55 °C) with time indicates the progress of blackberry formation. (inset) Calculation of the activation energy (E_a) for the blackberry formation. Reprinted with permission from ref. 53. Copyright 2005 American Chemical Society. (Right) Thermodynamic demonstration of the blackberry formation. Reprinted with permission from ref. 57. Copyright 2011 AAAS.

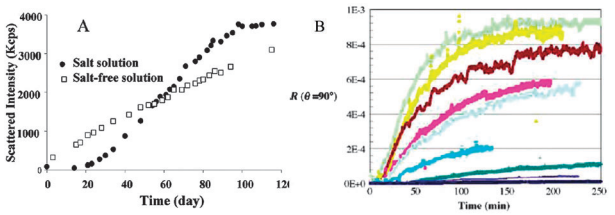

Fig. 13 (left) Comparison of scattered intensity increment (A) and R_h change (B) of two $\{Mo_{72}Fe_{30}\}$ samples along reaction time in 0.9 wt% NaCl and salt-free solutions Reprinted with permission from ref. 54. Copyright 2010 American Chemical Society. (right) Light scattering study of the assembly of HPV capsid proteins at various HPV concentrations. The lag time, reaction slope, and extent of assembly were dependent upon the initial protein concentration. Changes in scattered light were not observed until minutes later. Reprinted with permission from ref. 55. Copyright 2004 Elsevier.

To identify the oligomeric species during the lag period, sedimentation velocity (SV) experiments were performed on the 18th day after the $\{Mo_{72}Fe_{30}\}$ solution was prepared, corresponding to the final stage of the lag period in the kinetic curve (Fig. 14). In a typical SV experiment, the experimental curves were fitted using the Lamm equation to deduce the sedimentation coefficients (s) of sedimentating species and their corresponding sedimentation coefficient distributions $c(s)$ (Fig. 14). The results showed the coexistence of two species: $s \sim 6.6$ S with the dominant abundance (56%) and $s \sim 9.5$ S (10%), corresponding to $\{Mo_{72}Fe_{30}\}$ monomers and dimers, respectively. In addition, the measurement also suggested the possible existence of a small amount of larger oligomers (such as trimers) in solution. Besides the concentration of additional salts, the length of the lag period also depended on temperature, the valent state of the cations and the anions, as well as the solvent content.[54]

The assembly structures and formation processes of blackberries and virus capsids (mostly spherical, single-layered structures formed by the ordered assembly of capsid protein units which are also soluble macroanions) demonstrate interesting structural similarities. Furthermore, the sigmoidal curves suggested that both processes share similar mechanisms.[4,5] The hydrophobic interaction is widely believed as the dominant driving force for the virus capsid formation. However, for the POMs, they do not contain any hydrophobic moieties, and thus, hydrophobic interaction does not play a role in the blackberry formation. Then the question is: is it possible that the electrostatic interaction might be underestimated in the virus shell formation? Ideally and potentially, the POM macroions might be useful as simple model systems to study the more complicated bio-macromolecular systems.[4,42]

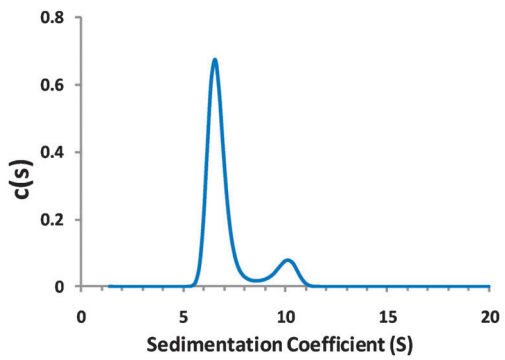

Fig. 14 Continuous size distribution $c(s)$ analysis of $\{Mo_{72}Fe_{30}\}$ solution *versus* sedimentation coefficient, s. Experiments were performed at a $\{Mo_{72}Fe_{30}\}$ concentration of 10 mg mL^{-1} in 170 mM NaCl solution at 20 °C. Reprinted with permission from ref. 54. Copyright 2010 American Chemical Society.

2.6. Permeability of the blackberry 'membrane' to small cations

Advanced AFM technology can realize *in situ* detection of blackberry structure in the solution state. A Si substrate was firstly modified with ammonium, which can positively charge the surface of the substrate under low pH. Then the substrate was immersed in the solution of $\{Mo_{72}Fe_{30}\}$ (water–acetone 50/50 vol%). Interestingly, ring-like structures were found when the AFM tip tapped the surface immersed in solution. The size of the ring was about the same as the size of assemblies observed from LLS studies. As time passed by, more and more 'rings' were detected, which was due to the comparatively slow adsorption of self-assembled structures on the surface. The AFM results confirmed that blackberries were negatively charged hollow structures and the shell of the sphere can be broken by AFM tips.[42]

As the *in situ* AFM results proved that the membranes of blackberry were quite soft, permeability tests indicated that the membranes selectively allowed cationic species to pass (Fig. 15).[56] The tests were based on the monitoring of fluorescence spectroscopy of water-soluble dyes that are specifically sensitive to one (or two) type of ions. Chlorotetracycline (CTC) (sensitive to Ca^{2+} and Mg^{2+}), 6-methoxyquinoline (6-MQ) (sensitive to Cl^-) and Coumarin 1 (sensitive to Br^-) were added to the freshly prepared $\{Mo_{72}Fe_{30}\}$ aqueous solution. The fluorophores would be partly incorporated into the inner space of blackberries during the self-assembly process, as confirmed by the 18 nm shift of their fluorescent signals. Specific ions sensitive to the dye were introduced into the solution after the completion of blackberry formation. A sudden jump in the fluorescence signal suggested that the

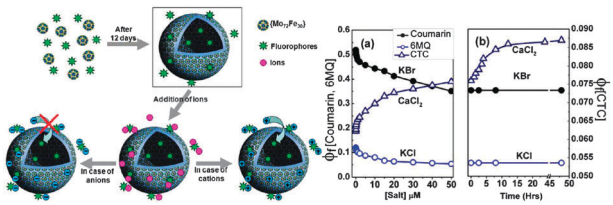

Fig. 15 (left) Formation of fluorophore-containing $\{Mo_{72}Fe_{30}\}$ blackberries in solution. The additional cations, once added into solution, instantly interact with fluorophores in bulk solution and on blackberry surfaces, subsequently enter into the blackberries, and interact with the fluorophores inside. The anions could not cross the membrane. (right) Change in fluorescence quantum yield of Coumarin 1,6-MQ, and CTC with addition of KBr, KCl, and $CaCl_2$, respectively; (a) instantaneous change occurs with the addition of salts; (b) change in fluorescence quantum yield with time, once the addition of salt is stopped. Reprinted with permission from ref. 56. Copyright 2008 American Chemical Society.

CTC molecules staying in bulk solution were immediately saturated after dominant amounts of Ca^{2+} ions were added. Interestingly, there was a very slow, continuous increment in the fluorescence signal after the initial process, suggesting a slow, continuous binding between Ca^{2+} ions and CTCs. The results could be explained as that Ca^{2+} ions could slowly pass the blackberry membranes and bind with CTC molecules inside. However, anions such as Cl^- and Br^- could not pass through the membrane.[56]

2.7. The self-recognition behavior during the self-assembly process

The POM macroions are good, simple models to understand some fascinating biological behaviors involving complex biomacromolecules. For example, self-recognition is a general and significant phenomenon in biological units directly connecting to many biological functions. It is important to understand the critical forces behind the self-recognition.[4,54]

A simple test is if POM macroions can self-recognize each other in a mixed solution during their self-assembly. The self-assemblies involving close-contact interactions (*e.g.* hydrophobic interactions) cannot achieve this, such as different types of surfactants usually form mixed micelles. In contrast, the blackberry formation is controlled by long-range, delicate electrostatic interactions. In the aqueous solutions containing the mixture of two spherical polyprotic "Keplerate" clusters: $\{Mo_{72}Fe_{30}\}$ and $\{Mo_{72}Cr_{30}\}$, both clusters have 30 characteristic and active $M(H_2O)$ groups coordinated to the non-Mo atoms, but different mobilities of their surface hydration layers as well as degrees of deprotonation. The water ligands (weak Brønsted acids) release protons, *i.e.*, about seven for $\{Mo_{72}Fe_{30}\}$ and about five for $\{Mo_{72}Cr_{30}\}$ in aqueous solution.[36]

The mixed aqueous solutions of $\{Mo_{72}Cr_{30}\}$ and $\{Mo_{72}Fe_{30}\}$ were studied to determine whether they form homogeneous or heterogeneous blackberry structures (Fig. 16). The two separated modes in the DLS study indicated the presence of two types of large species with different sizes (Fig. 17). The two peaks corresponded to those of the individual solutions containing either $\{Mo_{72}Cr_{30}\}$ or $\{Mo_{72}Fe_{30}\}$ at the same pH value. More convincing evidence for such self-recognition behavior could be obtained by individually analyzing the elements of the two assemblies corresponding to the two peaks. The two assemblies could be separated from the parent solution by filtration.[57]

As described in Section 2.5, the formation of oligomers is the rate-determining step for the blackberry formation. Time-resolved SLS studies at the early stage of the self-assembly (still in lag phase period) showed that the curves for the freshly prepared solutions of $\{Mo_{72}Cr_{30}\}$ and $\{Mo_{72}Fe_{30}\}$ were almost identical in slope and both show minor lag periods, suggesting that two dimer/oligomer formation processes in the solutions are kinetically similar. More importantly, SLS studies at both early stage and the whole self-assembly process indicated that the individual species assembled faster than their mixtures at a given concentration, which meant that the self-recognition started as early as the oligomer formation. The large energy barrier in the

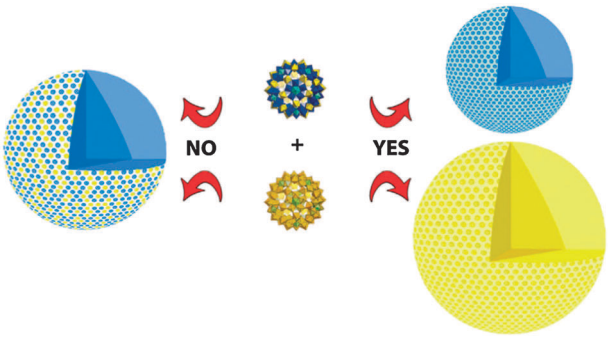

Fig. 16 (middle) In mixed dilute aqueous solutions, the clusters (polyhedral representation) $\{Mo_{72}Fe_{30}\}$ (top) and $\{Mo_{72}Cr_{30}\}$ (bottom) self-assemble into different (*i.e.* individual) blackberry structures of the Cr30 (yellow) and Fe30 type (blue)—with interfacial water between the macroions (right)—and do not form mixed species (such as the hypothetical structure shown on the left). Reprinted with permission from ref. 57. Copyright 2011 AAAS.

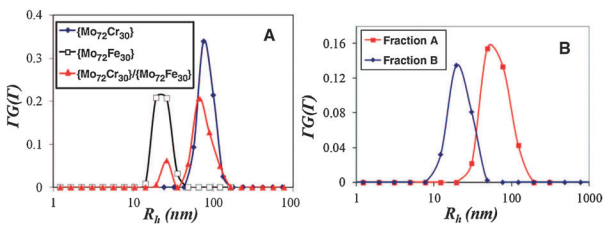

Fig. 17 (A) CONTIN analysis of the DLS studies at 90° scattering angle measured for aqueous solutions containing $\{Mo_{72}Cr_{30}\}$ or $\{Mo_{72}Fe_{30}\}$ (0.1 mg ml^{-1} each), as well as for a solution containing both species (0.1 mg ml^{-1} of each) (pH = 4.2). In the mixed solution, the peak due to the larger $\{Mo_{72}Cr_{30}\}$ assemblies is dominant because larger structures scatter more light. (B) CONTIN analysis of the DLS experiment carried out on the two components after ultrafiltration of the aqueous solution originally containing both $\{Mo_{72}Cr_{30}\}$ and $\{Mo_{72}Fe_{30}\}$ (0.1 mg ml^{-1} of each) by a series of membranes with different pore sizes; fraction A (red): material retained after filtering by 100 000 dalton-pore size membrane; fraction B (blue): material retained after filtering by 30 000 dalton-pore size membrane. Reprinted with permission from ref. 57. Copyright 2011 AAAS.

oligomer formation probably enabled the self-recognition even for species with minor differences. In the current case, the most critical factor of generating the self-recognition was due to the small charge density difference between these two types of macroions. Additionally, the 30 identical $Cr^{III}(H_2O)$ and $Fe^{III}(H_2O)$ groups differ greatly in the lability (*i.e.* residence time) of their water ligands. As a result, the interfacial water mobilities and heterogeneities of the macroions in the two superstructures differ significantly, and the hydrogen bonding network for the $\{Mo_{72}Cr_{30}\}$-type blackberries was more dense and stable. The different mobilities of the interfacial water networks can be confirmed by the fact that the transport of Ca^{2+} through the $\{Mo_{72}Cr_{30}\}$ blackberry membranes was slower than that through the $\{Mo_{72}Fe_{30}\}$-type system by a factor of 3 to 4.[57]

2.8. Theoretical studies on the polyoxoanionic solutions

Bo and Poblet *et al.* calculated the radial distribution functions of Li^+, Na^+, and K^+ with Keggin ions bearing 3-, 4-, and

5-charges, and the diffusion coefficients of these Keggins. The effect of the microscopic molecular details of the solvent was a key aspect to interpret the simulation results due to the competition between electrostatic interaction among the ions and the stability of the solvation shell. Further analysis showed that the solvent-shared structures weakly bound to the POM anions played a crucial role in the determination of the dynamic properties of the anions. The authors also suggested that the image of the ion pair as a well-defined molecular conformation had to be substituted by a more dynamic picture in which the paired ions moved inside the region bound by Bjerrum's length, with some preferred locations that were the result of the more stable balance between electrostatic interactions, entropic effects, as well as the solvent effect.[58,59]

Chaumont and Wipff performed theoretical simulations on the aggregation of Keggin anions ($PW_{12}O_{40}^{3-}$) in aqueous and methanol solutions. Aqueous solutions of Keggin anions were simulated at two anionic concentrations with Cs^+, NBu_4^+, UO_2^{2+}, Eu^{3+}, H_3O^+, and $H_5O_2^+$ being counterions, respectively (Fig. 18). They revealed a significant counterion effect related to the degree of salt dilution, as well as the cation–anion and anion–anion interactions. The hydrophobic NBu_4^+ cations tended to surround POMs *via* loose contacts and created a "phase separation" between water and a humid, salty, overall neutral domain where all ions were concentrated. For more hydrophilic cations, they were generally separated from the POM anions. The most important finding was the aggregation of POMs, mostly into dimers with short inter-POM distances (P···P < 12 Å), but also into oligomers in concentrated solutions where *ca.* 9 to 46% of the POMs formed aggregates, depending on the type of counterions. While Eu^{3+} and UO_2^{2+} were fully hydrated and interacted at short distances with POM anions as solvent-separated ion pairs, Cs^+ could form contact ion pairs, as well as solvent-separated ions. Among the monovalent counterions, $H_5O_2^+$ led to the most serious aggregation, due to the influence of the protons. The POMs' dynamic properties were also dependent on the counterions: their diffusion coefficients were the lowest with NBu_4^+, and highest with Cs^+, reflecting the degree of ion condensation in water. The role of water in the solution state of the POM salts was further demonstrated by simulating the most concentrated systems in methanol solution. Methanol solvated the counter-cations poorer than water did and could not form bridges between POMs, therefore a higher portion of anion–cation contacts, and no oligomers with short contacts could be found in methanol.[60]

Further detailed theoretical simulations were carried out to understand the like-charge attraction between Keggin type POMs. Wipff and co-workers calculated the changes in free energy $\Delta G(d)$ as a function of the P···P distance d, which represented the inter-POM distance. As the POM anions approached each other, the free energy profiles were found to be quite flat, with a tiny minimum at *ca.* 11 Å, showing that the anions can form "contact ion pairs" in the presence of either H_3O^+, UO_2^{2+} or Eu^{3+} counterions. The appearance of minimum energy around 10 Å and contact ion pairs were observed no matter what methodological variants were used, which supported the above finding that Keggin anions could form dimers or oligomers in water. The importance of stabilizing bridging water molecules was demonstrated by comparing the Keggin anion (PW^{3-}) to its spherical analogues (S^{3-}) and to Keggin cations (PW^{3+}, with all atomic charges of regular Keggin inverted) (Fig. 19a–c). The water bridged hydrogen bonds were specific in the dimer of Keggin anions, which were much stronger than the non-specific ones in the dimer of S^{3-}. Water could not afford bridging H-bonds with the cationic dimer but solvated the contact region of this dimer *via* its O_{H_2O} oxygens. The role of water was further demonstrated by

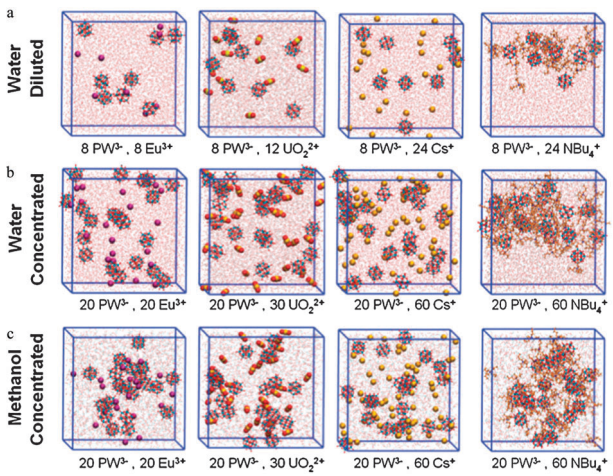

Fig. 18 Snapshots of the different simulation boxes after 10 ns. (a) Diluted aqueous solution; (b) concentrated aqueous solution; (c) concentrated methanol solution. Reprinted with permission from ref. 60. Copyright 2008 Royal Society of Chemistry.

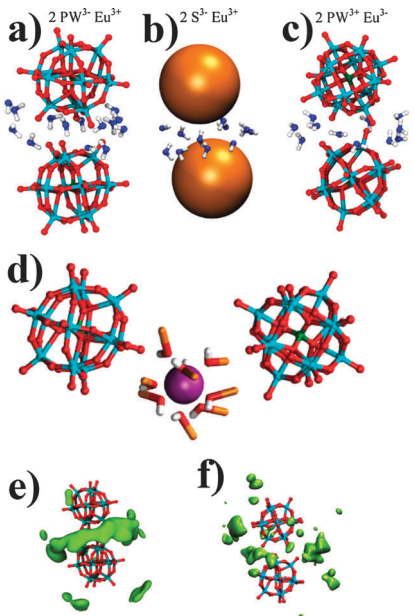

Fig. 19 (a), (b), (c) Snapshot of water molecules between 2 PW^{3-}, 2 S^{3-} or 2 PW^{3+} ions. (d) Snapshot of the $PW^{3-}\cdots Eu(MeOH)_9^{3+}\cdots PW^{3-}$ pair at a P···P distance of 17.5 Å, corresponding to the free energy minimum along the PMF in methanol. (e) and (f) Highest density region of Eu^{3+} and H_3O^+, respectively. Adapted with permission from ref. 61. Copyright 2012 Elsevier.

comparing the simulation results in water and in methanol solution where there was no contact ion pair, but a free energy minimum at *ca.* 17 Å, corresponding to an ion separated pair $PW^{3-}\cdots Eu(MeOH)_9^{3+}\cdots PW^{3-}$ (Fig. 19d). These findings were important for understanding processes like condensation and assembling of POMs and macroions in water or at aqueous interfaces. Analysis on the distribution of counterions around the Keggin-dimer structures revealed that the counterions were in the bridge area of the dimers and acted like a 'cationic glue' (Fig. 19e and f).[61]

Wipff's studies on comparatively small POMs confirmed the counterion-mediated attraction as a driving force and the existence of water-bridged hydrogen bonding interaction for like-charge attraction and further self-assembly behavior of macroions. Meanwhile, Kegel *et al.* claimed that only direct-contact hydrogen bonding contributed to the formation of POM shells while electrostatic repulsion played a role only in the folding of the sheet-like structures into a shell, based on a simplified model.[62] Their simulation results seemed to be inconsistent with the experimental results that the blackberry structures were disassembled into monomers without precipitation when $\{Mo_{72}Fe_{30}\}$ was uncharged (at pH < 2.9)[30] while the hydrogen bonding remained. Kegel's simulation would give opposite results, which could be due to the ignorance of the role of water molecules, such as the solvation effect of the macroions and the induced polarization of water molecules in their simulation. Secondly, the strength of hydrogen bonding is highly dependent on the deprotonation of the water ligands, the distance between donor (D) and acceptor (A) atoms and the D–H$\cdots$A angles, which require more complex models.

It might be difficult to do detailed simulations on giant POMs nowadays. Therefore, thermodynamic studies on the blackberry structures help reveal the key factor that might determine the size of blackberry structures. A simplified half empirical equation was presented by Kegel *et al.*[29] A charge-regulated self-assembly process was given to explain the formation of blackberry with a general expression for the blackberry radius R is expressed as

$$R \sim -48\lambda_B u/\psi^2 \qquad (1)$$

With $\lambda_B \sim 56/\varepsilon$. Consequently, the size of the blackberries is determined by three parameters: the solvent content (in ε), the effective charge on the blackberries (described by the zeta potential ψ), and the magnitude of the attractive force among the macroions (u).[29]

3. Self-assembly of covalently functionalized amphiphilic POM–organic hybrids

Chemical functionalization with organic components can effectively tune POMs' electronic structures and improve their compatibility and processability.[6] Due to their negative charges and the large amount of oxo ligands on their surfaces, POMs, generally speaking, are hydrophilic and therefore many of them are not compatible with organic media. Covalent functionalization by hydrophobic organic ligands renders the clusters amphiphilic features, which can be reflected in their self-assembly behavior in water/air and water/oil interface, polar and nonpolar solvents.[7–9,11–17,63]

Different from the self-assembly of macroions into blackberry structures, the driving force for the self-assembly of amphiphilic hybrid POMs is mostly solvophobic interaction. Being more complicated than the self-assembly of common amphiphilic surfactants, the study of the assembly of hybrid POMs needs to take the counterion effect and the bulky, charged polar head group into account besides the effects of molecular topology, solvent polarity, concentration, and hydrophobicity of the organic 'tails'.[7]

3.1. Surfactants with POMs as polar head groups

Conventional surfactants usually have one polar head group covalently linked with one or several hydrophobic (*e.g.* alkyl) tails. Packing parameter (P), defined from a surfactant's geometrical parameters, can be used to predict the assemblies of the surfactants in polar and nonpolar solvents.[7] The polar head groups of POM–organic hybrids have higher negative charge and much larger sizes. Our studies indicate that the POM-based hybrid surfactants show complicated but controllable self-assembly behavior.[12,63]

Due to the convenience in synthesis, the original counterions of the anionic polar head groups are usually bulky organic cations, such as tetrabutylammonium (TBA).[6] TBAs are strongly associated with polar head groups through static charge interaction in nonpolar solvents, which significantly reduces the polar heads' hydrophilic properties. Consequently, the amphiphilic properties of the hybrids are not obvious.[13] However, the association between TBAs and POM head groups becomes weaker when the solvent polarity is higher, which is confirmed by the difference in diffusion speed between TBA and anionic hybrids from NMR studies.[13] The hybrids show amphiphilic properties by self-assembling into vesicle structures in appropriate polar solvents (Fig. 20).[13] The vesicle sizes of S3 and S6 showed linear relationship with the inverse of the dielectric constant of the solvent, indicating a charge-regulated process. S3 showed a much more negative slope than that of S6, which could be related to the less negative charge of hexavanadate (V_6) (-2) compared to Dawson-type POM (-6).[13,63] The counterion disassociation is controlled by factors such as static charge interaction, solvent polarity and solvation of ions. Static charge force is proportional to the number of charges of the ions and thus, TBA could be easier to diffuse away from the surface of hexavanadates than from Dawsons (S6). Therefore, the effective charge on the S3 increases more significantly when the solvent polarity increases, which finally results in a more negative slope.[13,63] For S3, vesicles could only be observed when 20–35 vol% of

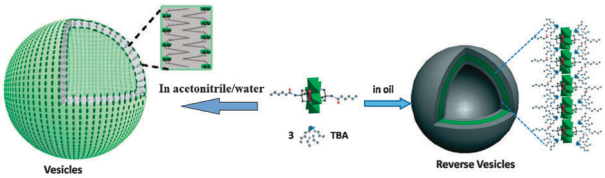

Fig. 20 The formation of vesicles and reverse vesicle structures in polar and nonpolar solvent, respectively. Adapted with permission from ref. 16 and 17. Copyright 2008 American Chemical Society and 2010 Wiley-VCH.

water was added to its acetone solution.[13] However, S6 can form vesicles in less polar solvents such as pure acetone.[13,63] Additionally, two of the hybrids (S1 and S2) were proved to be able to form reverse vesicles in nonpolar solvents (Fig. 20).[17] The sizes of the assemblies could be continuously increased by decreasing the polarities of the solvents, which is due to the increasing solvophobic interaction.[13,16]

Different salts soluble in acetonitrile, $ZnCl_2$, $CuCl_2$, NaI, tetrabutylammonium iodide (TBA·I) and dodecyltrimethylammonium bromide (DTMA·Br), were added to acetonitrile solutions of S6, respectively, to study the role of the counterions in the vesicle formation and vesicle size. The vesicle size decreased gradually with increasing concentration of $ZnCl_2$. Interestingly, the vesicle size remained unchanged at first upon addition of NaI, but gradually increased when the NaI concentration exceeds 0.03 mg mL^{-1}. $ZnCl_2$, which was quite solvated in acetonitrile, preferred coordinating to the terminal or bridging oxo ligands on the surface of the Dawson clusters, forcing the polar domains to be exposed to the solvent-environment, which in turn increased the curvature of the vesicles, *i.e.* the vesicle size became smaller. Upon the addition of NaI, on the other hand, the sodium ions contributed to shielding the high negative charges of the polar head groups from each other, and thus reduced the repulsion between the polar heads on the surface of the vesicle. The curvature of the vesicle decreased, and as a result the vesicle size increased. The additions of $CuCl_2$, TBA·I or DTMA·Br showed no obvious effect on the vesicle size as those cations were not able to replace the TBA cations that surrounded the polar Dawson clusters. However, TBA·I and DTMA·Br were observed to cause the disassembly of the vesicles.[63]

The hybrids can be water-soluble when the original counterions, TBAs, are replaced by protons through ion-exchange resin.[12,13] In aqueous solution, the POM head groups can work as nano-acid by reversibly releasing and associating protons with their surface oxo ligands. The assembly sizes were quite sensitive to pH of the aqueous solution. The increase in pH will further release the protons from the POM surface, which increases the net charges of the head groups. The resulting increasing repulsion between the POMs on the surface of vesicles increases the curvature of assemblies, *e.g.*, smaller vesicle sizes.[12,13]

Wang and co-workers were able to functionalized Dawson type POMs with polystyrene chain. They claimed that the hybrid aggregated into micro-spherical particles and precipitated from organic solvent when the Dawson polar head original counterions, TBAs, were replaced by proton through ion-exchange resin.[10] In the meantime, the surfactants with Keggin polar head groups were found by Polarz *et al.* to be able to self-assemble into micelles and lyotropic phases.[11] The surfactants were later observed to self-assemble into a hexagonal lattice at the air/water interface.[9]

3.2. Molecular bola from organic–inorganic hybrid POMs

Bola-amphiphiles are a type of molecules with a hydrophobic skeleton and two hydrophilic end groups. The synthetic technology rendered us the ability to apply Lindqvist and Dawson type POMs as the hydrophilic end groups (Fig. 21a and b).[8,15]

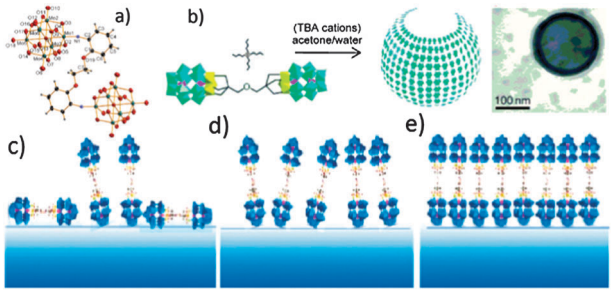

Fig. 21 (a) Molecular structure of hexamolybdate-based bola-amphiphiles. (b) Molecular structures of Dawson-type POMs-based bola-amphiphiles and their self-assembly into vesicle structures; monolayer formation for the dumbbell-shaped hybrid surfactants at the water/vapor interface: (c) liquid expansion (LE)/G phase, (d) LE phase, and (e) liquid condensed (LC) phase. Adapted with permission from ref. 8, 14, 15. Copyright 2010 American Chemical Society and 2009, 2011 Wiley-VCH.

By carefully tuning the polarity of solvents the bola-amphiphiles were observed to form bilayer vesicle structures with POMs on the outside surface while the organic linkers stayed inside the shell (Fig. 21b). The assembly size increased continuously with decreasing solvent polarity,[8,15] which showed the opposite trend with that of POM–organic hybrid surfactants. The vesicle formation was found to be an entropy-driven process, and the entropy term $T\Delta S$ was much larger compared with conventional surfactants, such as the ionic Gemini surfactants. In addition, the length of the organic linker might show a direct relation to the $T\Delta S$ value, as for a longer linker the entropy gain tended to be more negative because more hydrogen bonds needed to be broken.[14]

These Bola-amphiphilic hybrids also showed the formation of LB films at the air–water interface with TBA as counter-cations (Fig. 21c–e). The air/water interfacial behaviors, obtained from the π–A isotherms, for hybrids with linear alkyl chain linkers are relatively similar. However, hybrids with bipyridine and ether linkers present different air/water behavior. The liquid expanded and liquid condensed phases are clearly located and connected through a plateau. We believe that the hydrophobicity and composition of the organic linkers play dominant roles.[14]

3.3. Polymers containing POMs as building blocks

The conjugated polymers containing POM-terminal side chains that we studied in Section 2.4.3 can also be considered as amphiphiles in the nonpolar environment, under which circumstance all the charges on the POMs are neutralized.[44] The polymers show amphiphilic property in toluene since the polymer backbone is solvophilic while the POM clusters are solvophobic. DLS studies indicated the coexistence of two species with hydrodynamic radii (R_h) of *ca.* 5 ± 1 nm and 44 ± 3 nm, respectively, in the polymer's toluene solutions. The smaller species could be assigned as single polymer chains and the larger ones were likely assemblies. LLS results suggested a hollow spherical structure for the aggregates, which was also confirmed by TEM studies (Fig. 22). Interestingly, a large number of assemblies could be directly observed in solution under a fluorescence microscope as large dots. Based on the

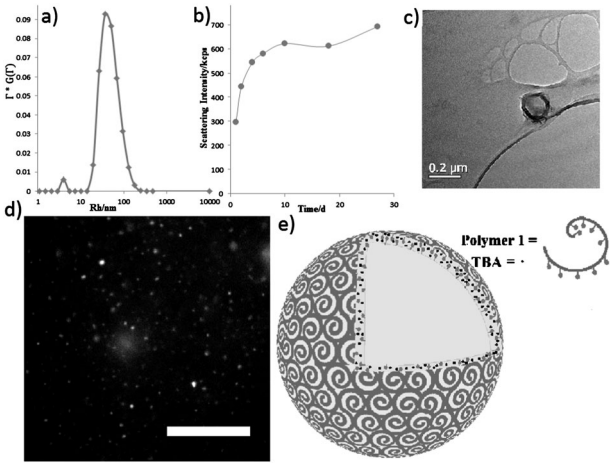

Fig. 22 (a) CONTIN analysis results of DLS data of polymer **1**'s 0.1 mg mL^{-1} toluene solution at a scattering angle of 30°; (b) the scattering intensities *versus* time monitored at 90° scattering angle for polymer **1**'s 0.1 mg mL^{-1} toluene solution. (c) TEM image of the assembly of polymer **1** in toluene. (d) Fluorescence microscope image of a 0.1 mg mL^{-1} toluene solution of polymer **1** (scale bar, 30 μm). (e) Model of the reverse vesicle structure in toluene. Reprinted with permission from ref. 44. Copyright 2012 Wiley-VCH.

analysis of the amphiphilic properties of **1**, the assemblies are presumed to be reverse vesicles with polymer backbones exposing to the solvent while the POMs forming the solvophobic interior (Fig. 22).[44]

3.4. Functionality and application of amphiphilic POM–organic hybrids

Being similar to the common amphiphiles, POM–organic hybrids were observed to be able to reduce the surface tension at the air/water interface. S3 shows a critical micelle concentration (CMC) of 0.23 mg mL^{-1}.[13] Furthermore, the surfactants with POMs as polar head groups could help forming stable emulsions in immiscible water–organic solvent systems.[11] Due to the high catalytic activity of POM polar head groups, the hybrid surfactants can work as emulsion catalysts in biphasic reaction systems.[64] Polarz *et al.* applied the surfactants with Keggin-type POM as polar head groups in the emulsion polymerization reaction environment. The route provided a convenient way to synthesize POM-based nano-scale catalytic particles.[11]

Another interesting feature is the controllable fluorescent properties of the hybrids' assemblies. Recently, Hill *et al.* synthesized two amphiphilic hybrids with two pyrene groups attached to the central polyoxovanadate, indicated as S5 in Table 3.[12] It was found that S5 could form fluorescent-active vesicular structures in water–DMSO mixed solvents by folding the pyrene groups into the middle hydrophobic layer.

Table 3 Formulas and molecular structures of the hybrid surfactants studied in our group

Abbreviation	Hybrid surfactants formula	Molecular structure
S1	$(TBA)_3[MnMo_6O_{18}\{(OCH_2)_3CNHCO(CH_2)_4CH_3\}_2]$	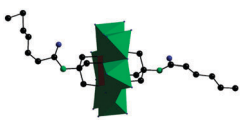
S2	$(TBA)_3[MnMo_6O_{18}\{(OCH_2)_3CNHCO(CH_2)_{14}CH_3\}_2]$	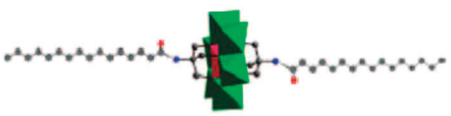
S3	$(TBA)_2[V_6O_{13}\{(OCH_2)_3CCH_2OOC(CH_2)_{16}CH_3\}_2]$	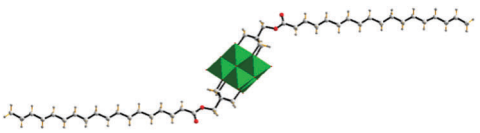
S4	$(TBA)_2[V_6O_{13}\{(OCH_2)_3CNHOC(CH_2)_3C_{16}H_9\}\{(OCH_2)_3CNH_2\}]$	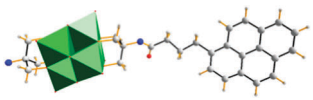
S5	$(TBA)_2[V_6O_{13}\{(OCH_2)_3CNHOC(CH_2)_3C_{16}H_9\}_2]$	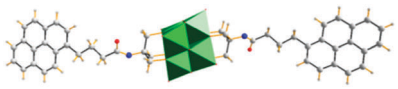
S6	$((TBA)_5H[P_2V_3W_{15}O_{59}(OCH_2)_3CNHCOC_{15}H_{31}]$	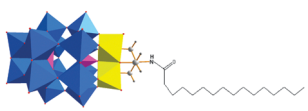
S7	$TBA_{10}H_2[\{P_2V_3W_{15}O_{59}(OCH_2)_3CNHCO\}_2]$	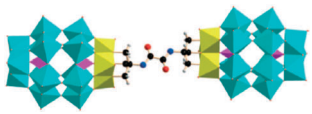

By replacing the original bulky TBA (TMA or TEA) counterions with protons, obvious emission peak shifts were noticed in the fluorescence spectra, which were attributed to the formation of pyrene excimers. Since it is well documented that the formation of pyrene excimers largely depends on spatial distance of two pyrene monomers (<0.5 nm), an estimation of the distance of adjacent S5 molecules could be made through monitoring the change of the emission pattern. Indeed, the emission spectra of pyrene gradually changed with the solution pH, and so did the vesicle size and effective charge. Moreover, from the 2D NOESY NMR study, for the first time, it was observed that the amphiphilic TBA counterions interact with pyrene groups in the hydrophobic layer of vesicles. This information is important to understand how the hybrid surfactants arrange themselves to form closely packed regions in the supramolecular structures and how the counter-ions perturb the solvent-phobic layer formation.[12]

4. Conclusion and outlook

The past decades have witnessed the significant advancement in the synthesis and application of POMs-based materials. Those large polyoxoanions represent the transitional area between simple ions and colloids, and are perfect models for understanding the solution behavior of polyelectrolytes. The macroions can further be applied to understand some biological phenomena such as the self-recognition behavior. Our further research will extend the study on the self-recognition behavior between polyoxoanions with tiny differences and the macroanions with anisotropic shapes or anisotropic charge distributions.

Meanwhile, the amphiphilic POM-based hybrids are novel surfactants with catalytic active polar head groups. Our studies suggest that the hybrids are able to form stable emulsions at the oil/water interface, which support the micro-environment for catalytic reactions of the POM polar head groups.

Acknowledgements

We gratefully acknowledge the support of this work by the NSF (CHE-1026505), Alfred P. Sloan Foundation, and Lehigh University.

Notes and references

1 C. L. Hill, *Chem. Rev.*, 1998, **98**, 1–2.
2 D.-L. Long, E. Burkholder and L. Cronin, *Chem. Soc. Rev.*, 2007, **36**, 105–121.
3 D.-L. Long, R. Tsunashima and L. Cronin, *Angew. Chem., Int. Ed.*, 2010, **49**, 1736–1758.
4 T. B. Liu, *Langmuir*, 2010, **26**, 9202–9213.
5 A. Zlotnick, J. M. Johnson, P. W. Wingfield, S. J. Stahl and D. Endres, *Biochemistry*, 1999, **38**, 14644–14652.
6 A. Dolbecq, E. Dumas, C. D. R. Mayer and P. Mialane, *Chem. Rev.*, 2010, **110**, 6009–6048.
7 D. Li, P. Yin and T. Liu, *Dalton Trans.*, 2012, **41**, 2853–2861.
8 F. Xiao, M. F. Misdrahi, J. Zhang, P. Yin, J. Hao, C. Lv, Z. Xiao, T. Liu and Y. Wei, *Chem.–Eur. J.*, 2011, **17**, 12006–12009.
9 J. J. Giner-Casares, G. Brezesinski, H. Möhwald, S. Landsmann and S. Polarz, *J. Phys. Chem. Lett.*, 2012, **3**, 322–326.
10 Y. Han, Y. Xiao, Z. Zhang, B. Liu, P. Zheng, S. He and W. Wang, *Macromolecules*, 2009, **42**, 6543–6548.
11 S. Landsmann, C. Lizandara-Pueyo and S. Polarz, *J. Am. Chem. Soc.*, 2010, **132**, 5315–5321.
12 D. Li, J. Song, P. Yin, S. Simotwo, A. J. Bassler, Y. Aung, J. E. Roberts, K. I. Hardcastle, C. L. Hill and T. Liu, *J. Am. Chem. Soc.*, 2011, **133**, 14010–14016.
13 P. Yin, P. Wu, Z. Xiao, D. Li, E. Bitterlich, J. Zhang, P. Cheng, D. V. Vezenov, T. Liu and Y. Wei, *Angew. Chem., Int. Ed.*, 2011, **50**, 2521–2525.
14 M. F. Misdrahi, M. Wang, C. P. Pradeep, F.-Y. Li, C. Lydon, L. Xu, L. Cronin and T. Liu, *Langmuir*, 2011, **27**, 9193–9202.
15 C. P. Pradeep, M. F. Misdrahi, F.-Y. Li, J. Zhang, L. Xu, D.-L. Long, T. Liu and L. Cronin, *Angew. Chem., Int. Ed.*, 2009, **48**, 8309–8313.
16 J. Zhang, Y.-F. Song, L. Cronin and T. Liu, *J. Am. Chem. Soc.*, 2008, **130**, 14408–14409.
17 J. Zhang, Y.-F. Song, L. Cronin and T. Liu, *Chem.–Eur. J.*, 2010, **16**, 11320–11324.
18 A. Müller, S. K. Das, V. P. Fedin, E. Krickemeyer, C. Beugholt, H. Bögge, M. Schmidtmann and B. Hauptfleisch, *Z. Anorg. Allg. Chem.*, 1999, **625**, 1187–1192.
19 A. Müller, E. Krickemeyer, H. Bögge, M. Schmidtmann and F. Peters, *Angew. Chem., Int. Ed.*, 1998, **37**, 3359–3363.
20 A. Müller and S. Roy, *Coord. Chem. Rev.*, 2003, **245**, 153–166.
21 A. Müller, S. Sarkar, S. Q. N. Shah, H. Bögge, M. Schmidtmann, S. Sarkar, P. Kögerler, B. Hauptfleisch, A. X. Trautwein and V. Schünemann, *Angew. Chem., Int. Ed.*, 1999, **38**, 3238–3241.
22 B. Botar, P. Kogerler and C. L. Hill, *Chem. Commun.*, 2005, 3138–3140.
23 R. C. Howell, F. G. Perez, S. Jain, J. W. DeW. Horrocks, A. L. Rheingold and L. C. Francesconi, *Angew. Chem., Int. Ed.*, 2001, **113**, 4155–4158.
24 S. S. Mal and U. Kortz, *Angew. Chem., Int. Ed.*, 2005, **44**, 3777–3780.
25 A. M. Todea, A. Merca, H. Bögge, J. van Slageren, M. Dressel, L. Engelhardt, M. Luban, T. Glaser, M. Henry and A. Müller, *Angew. Chem., Int. Ed.*, 2007, **46**, 6106–6110.
26 T. Liu, E. Diemann, H. Li, A. W. M. Dress and A. Müller, *Nature*, 2003, **426**, 59–62.
27 A. Müller, E. Diemann, C. Kuhlmann, W. Eimer, C. Serain, T. Tak, A. Knochel and P. K. Pranzas, *Chem. Commun.*, 2001, 1928–1929.
28 M. L. Kistler, A. Bhatt, G. Liu, D. Casa and T. Liu, *J. Am. Chem. Soc.*, 2007, **129**, 6453–6460.
29 A. A. Verhoeff, M. L. Kistler, A. Bhatt, J. Pigga, J. Groenewold, M. Klokkenburg, S. Veen, S. Roy, T. Liu and W. K. Kegel, *Phys. Rev. Lett.*, 2007, **99**, 066104.
30 T. B. Liu, B. Imber, E. Diemann, G. Liu, K. Cokleski, H. L. Li, Z. Q. Chen and A. Müller, *J. Am. Chem. Soc.*, 2006, **128**, 15914–15920.
31 M. J. Stevens, *Biophys. J.*, 2001, **80**, 130–139.
32 I. Sogami and N. Ise, *J. Chem. Phys.*, 1984, **81**, 6320–6332.
33 B. Chu and B. S. Hsiao, *Chem. Rev.*, 2001, **101**, 1727–1762.
34 J. M. Pigga, M. L. Kistler, C. Y. Shew, M. R. Antonio and T. B. Liu, *Angew. Chem., Int. Ed.*, 2009, **48**, 6538–6542.
35 J. M. Pigga, J. A. Teprovich, R. A. Flowers, M. R. Antonio and T. B. Liu, *Langmuir*, 2010, **26**, 9449–9456.
36 M. L. Kistler, T. B. Liu, P. Gouzerh, A. M. Todea and A. Müller, *Dalton Trans.*, 2009, 5094–5100.
37 A. Oleinikova, H. Weingärtner, M. Chaplin, E. Diemann, H. Bögge and A. Müller, *ChemPhysChem*, 2007, **8**, 646–649.
38 J. M. Pigga and T. Liu, *Inorg. Chim. Acta*, 2010, **363**, 4230–4233.
39 A. M. Todea, A. Merca, H. Bögge, T. Glaser, J. M. Pigga, M. L. K. Langston, T. Liu, R. Prozorov, M. Luban, C. Schröder, W. H. Casey and A. Müller, *Angew. Chem., Int. Ed.*, 2010, **49**, 514–519.
40 M. L. Kistler, K. G. Patel and T. B. Liu, *Langmuir*, 2009, **25**, 7328–7334.
41 P. P. Mishra, J. Jing, L. C. Francesconi and T. B. Liu, *Langmuir*, 2008, **24**, 9308–9313.
42 P. Yin, D. Li and T. Liu, *Isr. J. Chem.*, 2011, **51**, 191–204.
43 G. Liu, T. B. Liu, S. S. Mal and U. Kortz, *J. Am. Chem. Soc.*, 2006, **128**, 10103–10110.
44 P. Yin, L. Jin, D. Li, P. Cheng, D. V. Vezenov, E. Bitterlich, X. Wu, Z. Peng and T. Liu, *Chem.–Eur. J.*, 2012, **18**, 6754–6758.
45 B. B. Xu, M. Lu, J. H. Kang, D. Wang, J. Brown and Z. H. Peng, *Chem. Mater.*, 2005, **17**, 2841–2851.
46 M. J. Stevens, *Phys. Rev. Lett.*, 1999, **82**, 101–104.
47 F. Ribot, V. Escax, J. C. Martins, M. Biesemans, L. Ghys, I. Verbruggen and R. Willem, *Chem.–Eur. J.*, 2004, **10**, 1747–1751.

48 L. Van Lokeren, R. Willem, D. van der Beek, P. Davidson, G. A. Morris and F. Ribot, *J. Phys. Chem. C*, 2010, **114**, 16087–16091.
49 G. Liu, Y. G. Cai and T. B. Liu, *J. Am. Chem. Soc.*, 2004, **126**, 16690–16691.
50 G. Liu, M. L. Kistler, T. Li, A. Bhatt and T. B. Liu, *J. Cluster Sci.*, 2006, **17**, 427–443.
51 T. B. Liu, *J. Am. Chem. Soc.*, 2002, **124**, 10942–10943.
52 T. B. Liu, *J. Am. Chem. Soc.*, 2003, **125**, 312–313.
53 G. Liu and T. Liu, *Langmuir*, 2005, **21**, 2713–2720.
54 J. Zhang, D. Li, G. Liu, K. J. Glover and T. B. Liu, *J. Am. Chem. Soc.*, 2009, **131**, 15152–15159.
55 G. L. Casini, D. Graham, D. Heine, R. L. Garcea and D. T. Wu, *Virology*, 2004, **325**, 320–327.
56 P. P. Mishra, J. Pigga and T. Liu, *J. Am. Chem. Soc.*, 2008, **130**, 1548–1549.
57 T. Liu, M. L. K. Langston, D. Li, J. M. Pigga, C. Pichon, A. M. Todea and A. Müller, *Science*, 2011, **331**, 1590–1592.
58 F. Leroy, P. Miro, J. M. Poblet, C. Bo and J. B. Avalos, *J. Phys. Chem. B*, 2008, **112**, 8591–8599.
59 X. Lopez, C. Nieto-Draghi, C. Bo, J. B. Avalos and J. M. Poblet, *J. Phys. Chem. A*, 2005, **109**, 1216–1222.
60 A. Chaumont and G. Wipff, *Phys. Chem. Chem. Phys.*, 2008, **10**, 6940–6953.
61 A. Chaumont and G. Wipff, *C. R. Chim.*, 2012, **15**, 107–117.
62 E. Mani, J. Groenewold and W. K. Kegel, *Inorg. Chim. Acta*, 2010, **363**, 4295–4298.
63 P. Yin, C. P. Pradeep, B. Zhang, F.-Y. Li, C. Lydon, M. H. Rosnes, D. Li, E. Bitterlich, L. Xu, L. Cronin and T. Liu, *Chem.–Eur. J.*, 2012, **18**, 8157–8162.
64 P. Yin, J. Wang, Z. Xiao, P. Wu, Y. Wei and T. Liu, *Chem.–Eur. J.*, 2012, **18**, 9174–9178.